

## Equal channel angular extrusion of NiTi shape memory alloy tube

Shu-yong JIANG<sup>1</sup>, Ya-nan ZHAO<sup>1</sup>, Yan-qiu ZHANG<sup>1</sup>, Ming TANG<sup>1</sup>, Chun-feng LI<sup>2</sup>

1. Industrial Training Centre, Harbin Engineering University, Harbin 150001, China;

2. School of Materials Science and Engineering, Harbin Institute of Technology, Harbin 150001, China

Received 12 June 2012; accepted 18 December 2012

**Abstract:** As a new attempt, equal channel angular extrusion (ECAE) of nickel–titanium shape memory alloy (NiTi SMA) tube was investigated by means of process experiment, finite element method (FEM) and microscopy. NiTi SMA tube with the steel core in it was inserted into the steel can during ECAE of NiTi SMA tube. Based on rigid-viscoplastic FEM, multiple coupled boundary conditions and multiple constitutive models were used for finite element simulation of ECAE of NiTi SMA tube, where the effective stress field, the effective strain field and the velocity field were obtained. Finite element simulation results are in good accordance with the experimental ones. Finite element simulation results reveal that the velocity field shows the minimum value in the corner of NiTi SMA tube, where severe shear deformation occurs. Microstructural observation results reveal that severe plastic deformation leads to a certain grain orientation as well as occurrence of substructures in the grain interior and dynamic recovery occurs during ECAE of NiTi SMA tube. ECAE of NiTi SMA tube provides a new approach to manufacturing ultrafine-grained NiTi SMA tube.

**Key words:** NiTi tube; shape memory alloy; equal channel angular extrusion; severe plastic deformation; finite element method

### 1 Introduction

The remarkable attractiveness of nickel–titanium shape memory alloy (NiTi SMA) comes from its shape memory effect and superelasticity. Shape memory effect of NiTi SMA refers to its ability to recover original shape when being heated to the temperature above the austenite finish temperature ( $A_f$ ) after experiencing a certain deformation in the martensitic phase. Superelasticity of NiTi SMA refers to its nonlinear recoverable deformation behavior at temperatures above  $A_f$ , which is attributed to the stress-induced martensitic transformation under loading and the spontaneous reversion of the transformation under unloading [1–4].

NiTi SMA tube possesses a lot of excellent characteristics, such as kink resistance, crush resistance, flexibility, large recoverable deformation, high plateau stress and ultimate tensile strength, high potential energy storage capability, high fatigue life, outstanding superelastic behavior at or around the body temperature, so it has been one of the best candidates for the biomedical instruments so far [5–8]. However, NiTi SMA tube is difficult to process because of high strain

hardening and large elastic resilience. So far, the NiTi SMA tube has been mainly manufactured by the drawing processes, such as the hollow sinking, the fixed plug drawing, the floating plug drawing, the deformable mandrel drawing and the non-deformable mandrel drawing [9,10]. In addition to the drawing processes, the extrusion process was also used to manufacture the NiTi SMA tube [11].

Microstructures of NiTi SMA have a significant influence on its shape memory effect as well as superelasticity. In particular, grain refinement contributes to enhancing the functional properties and the mechanical properties of NiTi SMA. Severe plastic deformation (SPD) plays a significant role in microstructural refinement of NiTi SMA. As a SPD technique, equal channel angular extrusion (ECAE) is of great importance in refining the microstructures of NiTi SMA by means of large shear plastic strain. VALIEV et al [12,13] caused the microstructures of NiTi SMA to be refined down to 250 nm by means of ECAE and found that ECAE contributes to enhancing the yield strength, ultimate tensile strength, recoverable strain and maximum reaction stress. KOCKAR et al [14] obtained ultrafine-grained NiTi SMA with the average

grain size of 100 nm via ECAE, and found that ECAE results in the occurrence of (011) compound twins in addition to  $\langle 011 \rangle$  II type and  $\{11\bar{1}\}$  I type twins in the martensitic microstructures at room temperature, and leads to a considerable improvement in the thermal stability of phase transformation temperatures and thermal hysteresis as well as an increase in the critical stress level for dislocation slip due to grain size refinement. ECAE of NiTi SMA at high temperatures such as 1123 K and 1023 K has been investigated and the grain refinement is insufficient and dynamic recovery occurs rather than dynamic recrystallization during ECAE at high temperatures [15,16]. The two-step phase transformations in the ECAE-processed NiTi sample such as  $B2 \rightarrow R \rightarrow B19'$  upon cooling and  $B19' \rightarrow R \rightarrow B2$  upon heating have been reported [17,18].

So far, how to manufacture the ultrafine-grained NiTi SMA tube has never been reported in the literatures. In the present study, ECAE of NiTi SMA tube is preliminarily investigated by means of the process experiments, finite element method (FEM) and microscopy.

## 2 Experimental

### 2.1 Fundamentals of ECAE

The schematic diagram of ECAE of NiTi SMA tube is shown in Fig. 1. The NiTi SMA tube in which the steel core is placed is inserted into the steel can and is sealed by means of the NiTi plug. According to the fundamentals of ECAE of the bulk metal material, the steel can with the NiTi SMA tube in it is placed into the ECAE die and then is imparted to SPD which leads to the grain refinement of the NiTi SMA tube. In the study, the cross-section of the steel can is selected as the square. The channel angle is determined as  $120^\circ$ .

### 2.2 Experimental materials

The NiTi SMA tube sample for ECAE is shown in

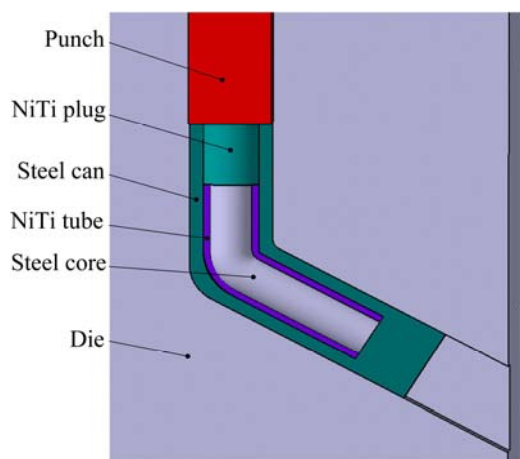


Fig. 1 Schematic diagram of ECAE of NiTi SMA tube

Fig. 2. The NiTi SMA tube, which possesses the inner diameter of 3 mm, the wall thickness of 0.5 mm and the height of 15 mm, was fabricated from the NiTi SMA bar with the diameter of 12 mm by means of electro-discharge machining (EDM). The NiTi SMA bar with a nominal composition of  $\text{Ni}_{50.9}\text{Ti}_{49.1}$  (mole fraction, %) was prepared by vacuum induction melting method before it was rolled at  $800^\circ\text{C}$ , and finally was drawn to the NiTi bar at  $400^\circ\text{C}$ . As a sealed part, the NiTi plug with the diameter of 4 mm and the height of 5 mm was also fabricated from the NiTi SMA bar. The steel can and the steel core were made of low carbon steel. The steel can had a square cross-section of  $6\text{ mm} \times 6\text{ mm}$  and a height of 25 mm. Furthermore, there was a blind hole with the inner diameter of 4 mm and the height of 20 mm in the steel can. The steel core possessed the diameter of 3 mm and the height of 15 mm. The lubricant was coated between the steel core and the NiTi SMA tube as well as between the steel can and the NiTi tube in order to make it easy to remove the NiTi SMA tube after ECAE. The original microstructure of the NiTi SMA tube before ECAE is shown in Fig. 3, where the original microstructure of the NiTi SMA tube belongs to the equiaxed grains.

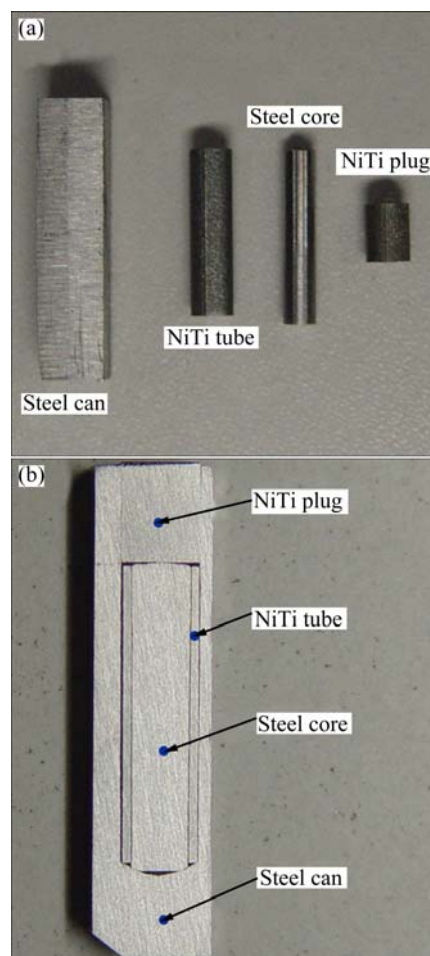


Fig. 2 Schematic diagram of NiTi SMA tube samples for ECAE: (a) Unassembled parts; (b) Assembled sample (section)

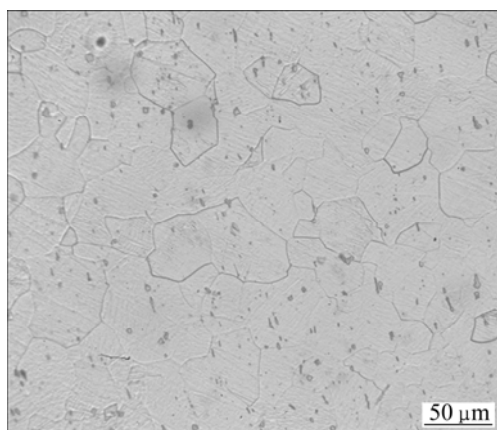


Fig. 3 Optical microstructure of original NiTi SMA tube

### 2.3 ECAE process

The assembled NiTi SMA tube samples were placed into the ECAE die and then they were put into the Instron–5500R universal testing machine, where the assembled SMA NiTi tube samples were heated to 500 °C. Subsequently, the pressing punch moved down at the speed of 1 mm/s. Consequently, the assembled SMA NiTi tube samples were forced to go across the channel of the die and thus the ECAE process was finished.

### 2.4 Compression test

The NiTi SMA samples with the diameter of 4 mm and the height of 6 mm were prepared from the NiTi SMA bar whose state was identical to the NiTi SMA tube for ECAE and were used for compression test in order to obtain the constitutive model of the NiTi SMA. In the same manner, the steel samples with the diameter of 4 mm and the height of 6 mm were prepared from the low carbon steel used for the steel can and the steel core for ECAE and were used for compression test in order to obtain the involved constitutive model. The compression experiments were carried out on the Instron–5500R universal testing machine at the strain rates ranging from 0.001 s<sup>-1</sup> to 1 s<sup>-1</sup> and at 500 °C.

### 2.5 Microstructural observation

The microstructures of the compressed NiTi SMA samples as well as the NiTi SMA tubes before ECAE and after ECAE were observed by means of optical microscopy. All the specimens for optical microscopy were etched in a solution of 10% HF + 40% HNO<sub>3</sub> + 50% H<sub>2</sub>O.

## 3 Finite element simulation of ECAE of NiTi SMA tube

### 3.1 Constitutive model

Establishing the appropriate constitutive model of

NiTi SMA plays a significant role in simulating ECAE of the NiTi SMA tube. Figure 4 demonstrates the stress—strain curves of NiTi SMA at 500 °C and the strain rates of 0.001, 0.01, 0.1 and 1 s<sup>-1</sup>, respectively. It can be seen from Fig. 4 that the true stress of NiTi SMA increases with increasing the strain rate, which indicates that NiTi SMA is sensitive to the strain rates and thus belongs to rigid-viscoplastic materials at 500 °C. Figure 5 shows the microstructures of the involved compressed samples at different strain rates, which reveal that NiTi SMA is obviously characterized by dynamic recovery at all the strain rates instead of dynamic recrystallization. Therefore, ECAE of NiTi SMA tube was carried out at 500 °C. The constitutive model of NiTi SMA in Fig. 4 shall be used as the material model in subsequent finite element simulation of ECAE of NiTi SMA tube. The true stress—strain curves of the low carbon steel for the steel can and the steel core at 500 °C are illustrated in Fig. 6 and are used as the material model of the steel can and the steel core during ECAE of NiTi SMA tube. Therefore, multiple constitutive models including NiTi SMA tube, NiTi plug, steel can and steel core are applied during ECAE of NiTi SMA tube.

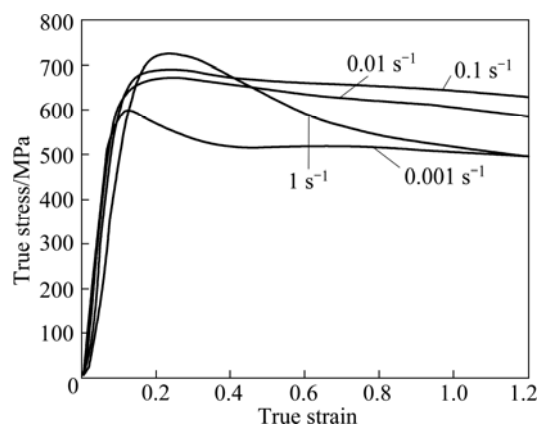
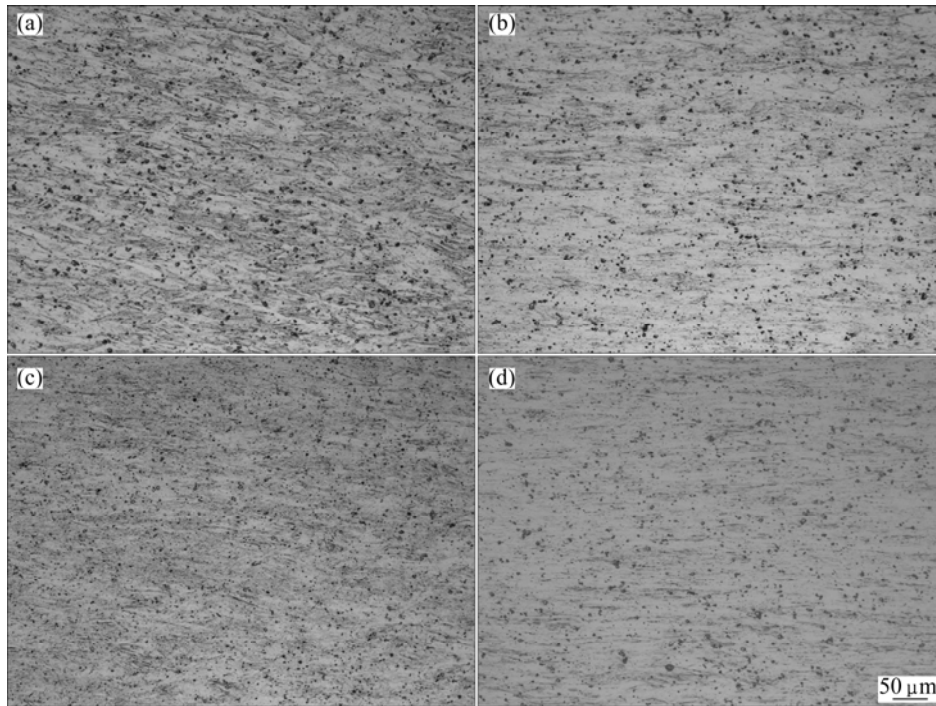


Fig. 4 Stress—strain curves of NiTi SMA at 500 °C

### 3.2 Finite element model

DEFORM3D finite element code was used to simulate ECAE of NiTi shape memory alloy tube. Figure 7 indicates the finite element model of ECAE of NiTi SMA tube. It can be seen from Fig. 7 that the boundary conditions are very complicated and there exist multiple coupled boundary conditions, such as between NiTi tube and steel core, between NiTi tube and steel can, between NiTi plug and steel can, between NiTi plug and NiTi tube, between NiTi plug and steel core, between steel core and steel can, between steel can and die, between steel can and punch and between NiTi plug and punch. According to the ECAE process parameters, the pressing speed of the punch is selected as 1 mm/s, and the pressing stroke of the punch is determined as 20 mm during the finite element simulation.



**Fig. 5** Microstructures of compressed samples of NiTi SMA at 500 °C and different strain rates: (a)  $0.001 \text{ s}^{-1}$ ; (b)  $0.01 \text{ s}^{-1}$ ; (c)  $0.1 \text{ s}^{-1}$ ; (d)  $1 \text{ s}^{-1}$

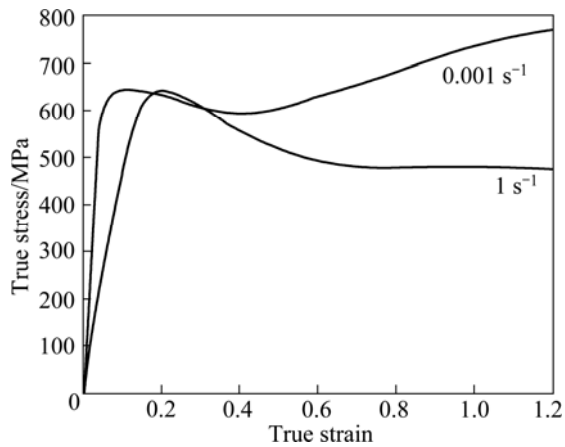


**Fig. 6** Stress—strain curves of low carbon steel at 500 °C

### 3.3 Finite element simulation results

Figure 8 shows the finite element simulation results of ECAE of NiTi SMA tube along with steel can and steel core, where the effective stress field, the effective strain field and the velocity field are obtained. Simultaneously, NiTi SMA tube is separated from the finite element simulation results in order to better understand the deformation mechanism of ECAE of NiTi SMA tube, as shown in Fig. 9. It can be seen from the effective stress field that the effective stress distributes uniformly along the cross-section of NiTi SMA tube and possesses the maximum value in the inner and outer corner. Three-dimensional compressive stress in the deformation zone contributes to enhancing plasticity of

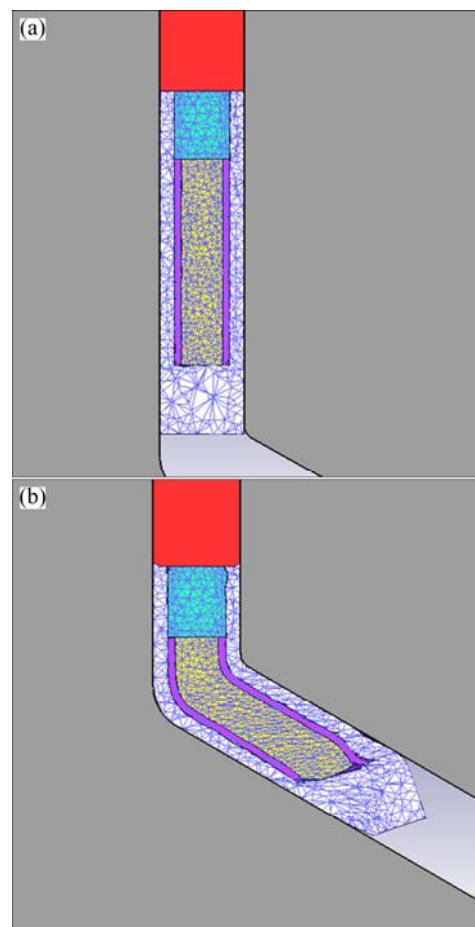


**Fig. 7** Finite element model of ECAE of NiTi SMA tube: (a) Before deformation; (b) After deformation

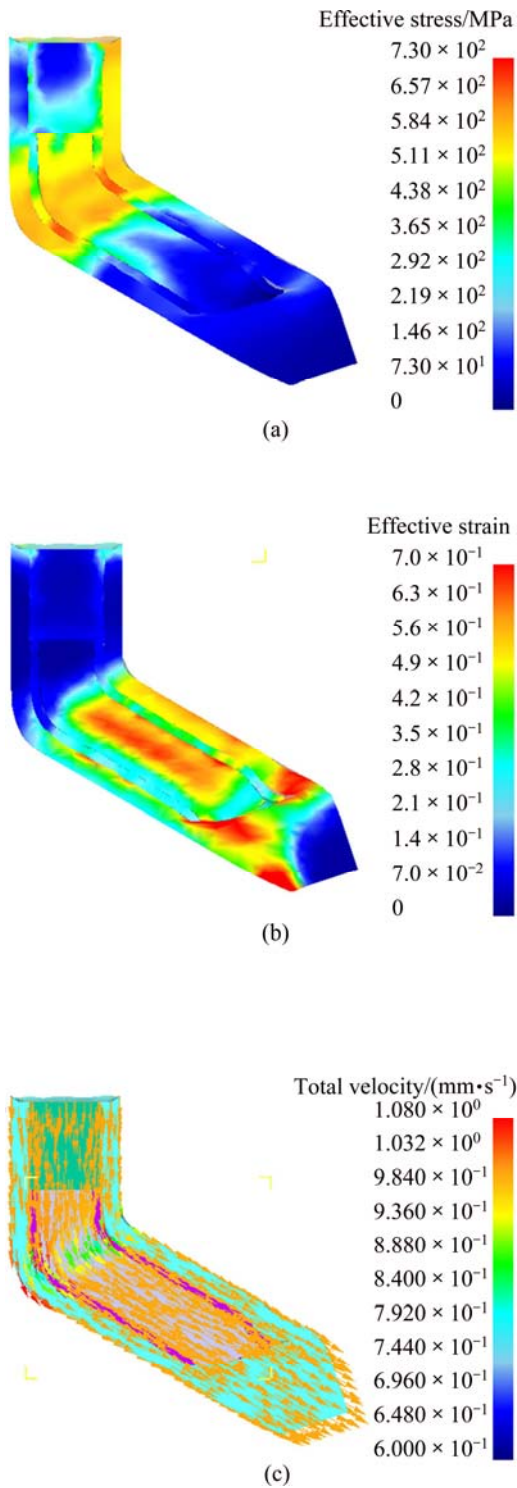


**Fig. 8** Finite element simulation results of ECAE of NiTi SMA tube along with steel can and steel core: (a) Effective stress field; (b) Effective strain field; (c) Velocity field

NiTi SMA tube. However, the effective strain field indicates that the effective strain distributes unevenly along the cross-section of NiTi SMA tube. It is evident that the effective strain value in the inner corner is greater than that in the outer corner. It can be seen from the velocity field that material particles flow uniformly

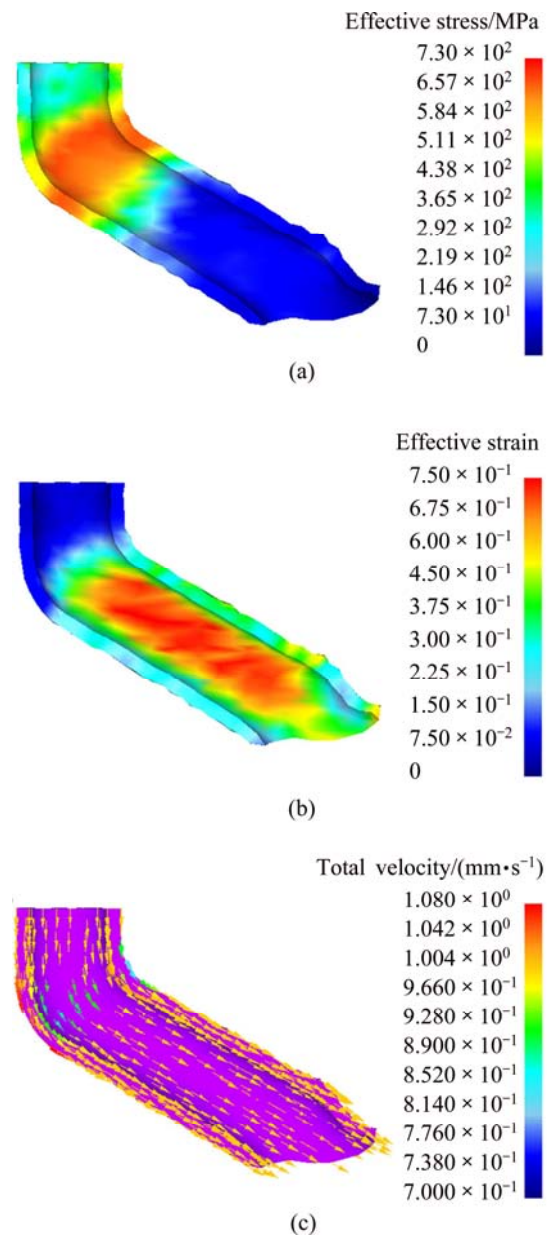


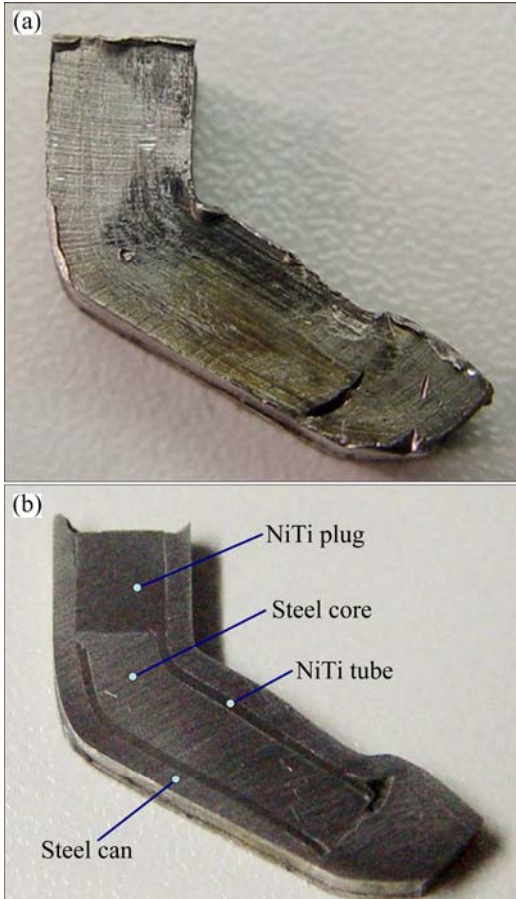
**Fig. 9** Finite element simulation results of ECAE of single NiTi SMA tube: (a) Effective stress field; (b) Effective strain field; (c) Velocity field

except those in the corner of NiTi SMA tube. Furthermore, the velocity value of the material particles in the corner of NiTi SMA tube is obviously lower than that in the other zones. The phenomenon indicates that so severe shear deformation occurs in the corner of NiTi SMA tube that the flow of material particles is impeded in the corner of NiTi SMA tube.

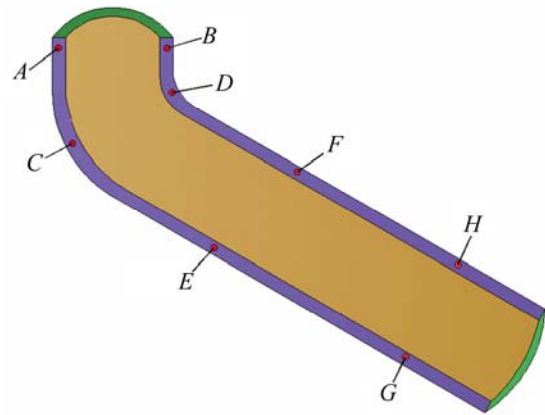
#### 4 Microstructures of ECAE-processed NiTi SMA tube

Figure 10 shows the sample obtained by means of ECAE process experiment. Only one pass of extrusion

was performed in order to investigate the deformation law of ECAE of NiTi SMA tube. It can be obviously seen from Fig. 10 that the experimental results agree well with the finite element simulation ones. NiTi SMA tube is divided into various zones in order to investigate the influence of ECAE on microstructures of NiTi SMA tube, as shown in Fig. 11. Figure 12 shows the microstructures of all the marked zones in NiTi SMA tube in Fig. 11. It can be found from Figs. 12 (a) and (b) that, compared with the original microstructure of NiTi SMA tube, the microstructure in zone A in Fig. 11 shows no too much difference, but plenty of substructures occur in the grains in zone B in Fig. 11. The phenomenon indicates that larger plastic deformation takes place in zone B than in zone A, and material particles in zone B are subjected to plastic deformation more quickly than those in zone A. It can be also found from Figs. 12 (c) and (d) that the microstructures in zone C as well as in zone D are characterized by intracrystalline stripes, which show a certain orientation. Zones C and D belong to the zones which are undergoing severe shear deformation. Furthermore, a higher density of substructures arise in zone D than in zone C, which indicates that plastic deformation is larger in the inner corner of NiTi SMA tube than in the outer corner of NiTi SMA tube.



**Fig. 10** Sample subjected to ECAE: (a) Integral structure; (b) Longitudinal section



**Fig. 11** Schematic diagram of deformation zones in NiTi SMA tube subjected to ECAE

Similarly, intracrystalline stripes occur in the grains in zones E and F which belong to deformed zones and are characterized by a certain orientation as well. It seems that dynamic recovery occurs during ECAE of NiTi SMA tube [12,13]. However, it is interesting that there are no intracrystalline stripes in zones G and H which belong to deformed zones likewise. The phenomenon is attributed to the occurrence of static recovery during ECAE of NiTi SMA tube. Compared with the other zones, zones G and H experience a longer recovery time, and plastic deformation work and frictional work lead to temperature rise in zones G and H, which provides a sufficient energy to eliminate the substructures in the grains. Certainly, the nature of the intracrystalline stripes shall further be investigated in the future work.

## 5 Conclusions

1) Multiple coupled boundary conditions and multiple constitutive models were used for finite element simulation of ECAE of NiTi SMA tube. Finite element simulation results are in good accordance with the experimental ones. ECAE of NiTi SMA tube provides a new approach to manufacturing ultrafine-grained NiTi SMA tube.

2) The effective stress field, the effective strain field and the velocity field were obtained by means of finite element simulation of ECAE of NiTi SMA tube. The effective strain field indicates that plastic deformation in the inner corner is greater than that in the outer corner. The velocity field indicates that the flow of material particles is impeded in the corner during ECAE of NiTi SMA tube.

3) ECAE of NiTi SMA tube leads to the orientation of the grains as well as the occurrence of the substructures in the grain interior. Furthermore, the dynamic recovery occurs during ECAE of NiTi SMA tube.

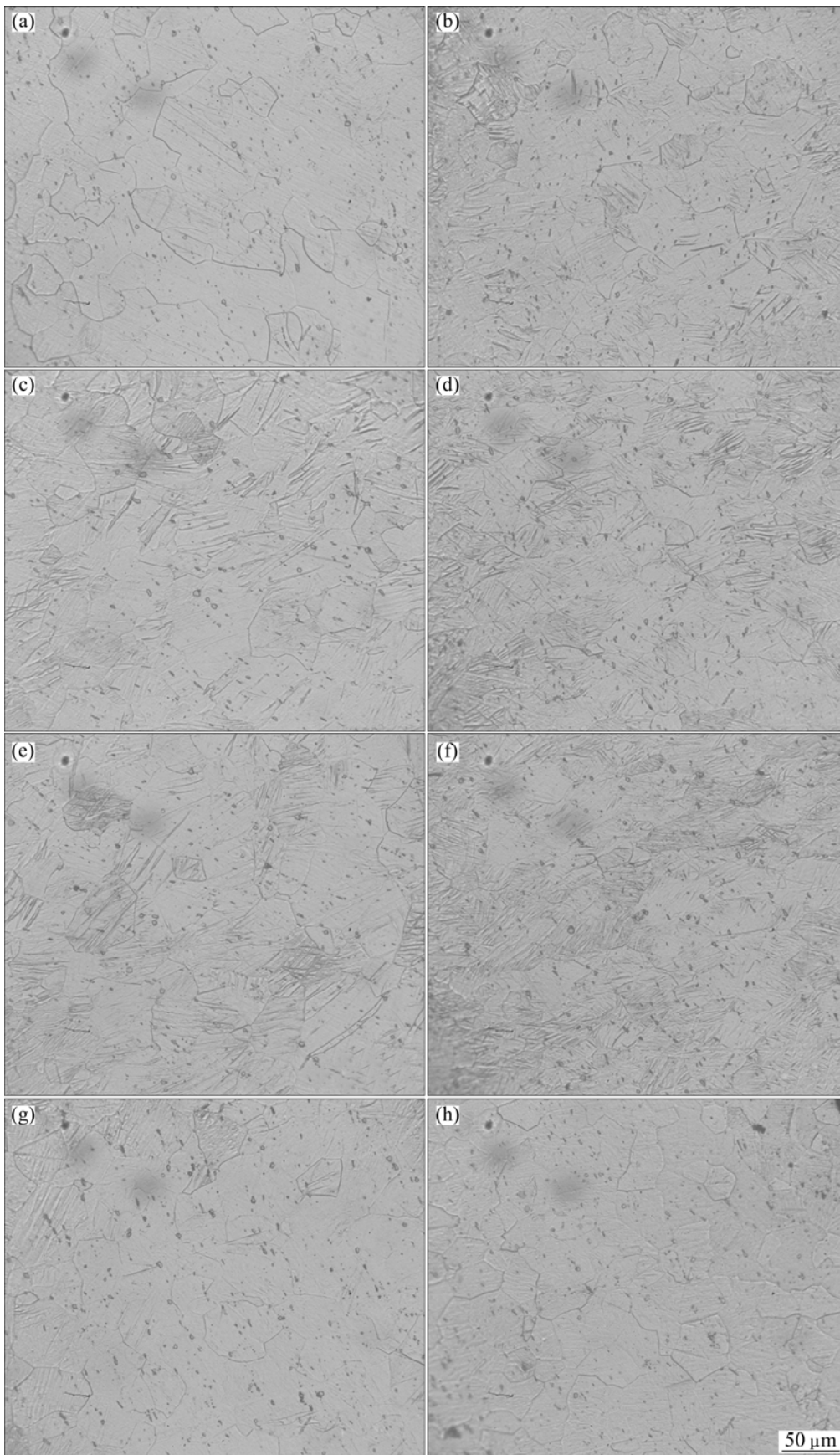


**Fig. 12** Optical microstructures of NiTi SMA tube subjected to ECAE deformation zones shown in Fig. 11: (a) Zone A; (b) Zone B; (c) Zone C; (d) Zone D; (e) Zone E; (f) Zone F; (g) Zone G; (h) Zone H

Microstructural refinement of NiTi SMA tube is not very significant due to only one pass of extrusion. Multi-pass ECAE of NiTi SMA tube shall be investigated in the future work.

## References

- [1] OTUKA K, REN X. Physical metallurgy of Ti–Ni-based shape memory alloys [J]. Progress in Materials Science, 2005, 50(5): 511–678.
- [2] JIANG Shu-yong, ZHANG Yan-qiu. Microstructure evolution and deformation behavior of as-cast NiTi shape memory alloy under compression [J]. Transactions of Nonferrous Metals of Society of China, 2012, 22(1): 90–96.
- [3] JIANG Shu-yong, ZHANG Yan-qiu, FAN Hong-tao. Fracture behavior and microstructure of as-cast NiTi shape memory alloy [J]. Transactions of Nonferrous Metals of Society of China, 2012, 22(6): 1401–1406.
- [4] ZHANG Yan-qiu, JIANG Shu-yong, ZHAO Ya-nan, TANG Ming. Influence of cooling rate on phase transformation and microstructure of Ti–50.9%Ni shape memory alloy [J]. Transactions of Nonferrous Metals of Society of China, 2012, 22(11): 2685–2690.
- [5] LI Z Q, SUN Q P. The initiation and growth of macroscopic martensite band in nano-grained NiTi microtube under tension [J]. International Journal of Plasticity, 2002, 18(11): 1481–1498.
- [6] ROBERTSON S W, RITCHIE R O. In vitro fatigue-crack growth and fracture toughness behavior of thin-walled superelastic Nitinol tube for endovascular stents: A basis for defining the effect of crack-like defects [J]. Biomaterials, 2007, 28(4): 700–709.
- [7] NG K L, SUN Q P. Stress-induced phase transformation and detwinning in NiTi polycrystalline shape memory alloy tubes [J]. Mechanics of Materials, 2006, 38(1–2): 41–56.
- [8] HE Y J, SUN Q P. Scaling relationship on macroscopic helical domains in NiTi tubes [J]. International Journal of Solids and Structures, 2009, 46(24): 4242–4251.
- [9] YOSHIDA K, WATANABE M, ISHIKAWA H. Drawing of Ni–Ti shape-memory-alloy fine tubes used in medical tests [J]. Journal of Materials Processing Technology, 2001, 118(1–3): 251–255.
- [10] YOSHIDA K, FURUYA H. Mandral drawing and plug drawing of shape-memory-alloy fine tubes used in catheters and stents [J]. Journal of Materials Processing Technology, 2004, 153–154: 145–150.
- [11] MÜLLER K. Extrusion of nickel–titanium alloys Nitinol to hollow shapes [J]. Journal of Materials Processing Technology, 2001, 111(1–3): 122–126.
- [12] VALIEV R Z, LANGDON T G. Principles of equal-channel angular pressing as a processing tool for grain refinement [J]. Progress in Materials Science, 2006, 51(7): 881–981.
- [13] PUSHIN V G, STOLYAROV V V, VALIEV R Z, LOWE T C, ZHU Y T. Nanostructured TiNi-based shape memory alloys processed by severe plastic deformation [J]. Materials Science and Engineering A, 2005, 410–411: 386–389.
- [14] KOCKAR B, KARAMAN I, KIM J I, CHUMLYAKOV Y I, SHARP J, YU C J. Thermomechanical cyclic response of an ultrafine-grained NiTi shape memory alloy [J]. Acta Materialia, 2008, 56(14): 3630–3646.
- [15] LI Z H, CHENG X H, SHANGGUAN Q Q. Effects of heat treatment and ECAE process on transformation behaviors of TiNi shape memory alloy [J]. Materials Letters, 2005, 59(6): 705–709.
- [16] LI Z H, XIANG C Q, CHENG X H. Effects of ECAE process on microstructure and transformation behavior of TiNi shape memory alloy [J]. Materials & Design, 2006, 27(4): 324–328.
- [17] FAN Z G, XIE C Y. Phase transformation behaviors of Ti–50.9at.% Ni alloy after equal channel angular extrusion [J]. Materials Letters, 2008, 62(6–7): 800–803.
- [18] ZHANG X N, SONG J, HUANG C L, XIA B Y, CHEN B, SUN X G, Xie C Y. Microstructures evolution and phase transformation behaviors of Ni-rich TiNi shape memory alloys after equal channel angular extrusion [J]. Journal of Alloys and Compounds, 2011, 509(6): 3006–3012.

## 镍钛形状记忆合金管的等通道转角挤压

江树勇<sup>1</sup>, 赵亚楠<sup>1</sup>, 张艳秋<sup>1</sup>, 唐明<sup>1</sup>, 李春峰<sup>2</sup>

1. 哈尔滨工程大学 工程训练中心, 哈尔滨 150001;

2. 哈尔滨工业大学 材料科学与工程学院, 哈尔滨 150001

**摘要:** 作为一种新的尝试, 将工艺实验、有限元法和显微分析技术相结合, 研究镍钛形状记忆合金管的等通道转角挤压。在等通道转角挤压过程中, 镍钛形状记忆合金管内部装有钢芯, 然后将其封装在钢套中。基于刚粘塑性有限元法, 镍钛形状记忆合金管等通道转角挤压的有限元模拟采用多种耦合边界条件和多种本构模型。通过有限元模拟, 获得了镍钛形状记忆合金管等通道转角挤压的等效应力场、等效应变场和速度场。有限元模拟结果和实验结果具有很好的一致性。有限元模拟结果表明, 在镍钛形状记忆合金管的转角处, 速度场具有最小值, 发生大剪切变形。显微组织观察结果表明, 在镍钛形状记忆合金管的等通道转角挤压期间, 大塑性变形导致晶粒具有一定的取向性, 在晶内产生亚结构, 并有动态回复发生。等通道转角挤压为制备超细晶镍钛形状记忆合金管提供了一种新的途径。

**关键词:** 镍钛管材; 形状记忆合金; 等通道转角挤压; 大塑性变形; 有限元法

(Edited by Hua YANG)